NANO LETTERS

Letter

pubs.acs.org/NanoLett

Anticorrelation of Photoluminescence from Gold Nanoparticle Dimers with Hot-Spot Intensity

Dmitry Sivun, Cynthia Vidal, Battulga Munkhbat, Nikita Arnold, Thomas A. Klar, and Calin Hrelescu*

Institute of Applied Physics, Johannes Kepler University Linz, 4040 Linz, Austria

Supporting Information

ABSTRACT: Bulk gold shows photoluminescence (PL) with a negligible quantum yield of ~10^{-10}, which can be increased by orders of magnitude in the case of gold nanoparticles. This bears huge potential to use noble metal nanoparticles as fluorescent and unbleachable stains in bioimaging or for optical data storage. Commonly, the enhancement of the PL yield is attributed to nanoparticle plasmons, specifically to the enhancements of scattering or absorption cross sections. Tuning the shape or geometry of gold nanostructures (e.g., via reducing the distance between two nanoparticles) allows for redshifting both the scattering and the PL spectra. However, while the scattering cross section increases with a plasmonic redshift, the PL yield decreases, indicating that the common simple picture of a plasmonically boosted gold luminescence needs more detailed consideration. In particular, precise experiments as well as numerical simulations are required. Hence, we systematically varied the distance between the tips of two gold bipyramids on the nanometer scale using AFM manipulation and recorded the PL and the scattering spectra for each separation. We find that the PL intensity decreases as the interparticle coupling increases. This anticorrelation is explained by a theoretical model where both the gold-intrinsic d-band hole recombination probabilities as well as the field strength inside the nanostructure are considered. The scattering cross section or the field strength in the hot-spot between the tips of the bipyramids are not relevant for the PL intensity. Besides, we not only observe PL supported by dipolar plasmon resonances, but also measure and simulate PL supported by higher order plasmonic modes.

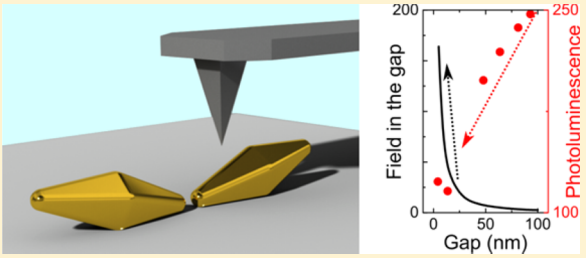

KEYWORDS: *Gold nanoparticles, photoluminescence, AFM-manipulation, plasmonics, hot-spot, field enhancement*

Photoluminescence (PL) from bulk gold or a smooth gold film (Figure 1) is attributed to a multistep process (Figure 1, inset):[1−3] electrons are excited by 405 nm photons from the d-band into the sp-band, followed by a scattering of the hole in the d-band to some point in k-space with filled sp-electronic states below the Fermi level, from where this hole can recombine with an sp-band electron. Both steps, scattering within the d-band and recombination, are prone to losses and hence the overall quantum yield is in the range of ~10^{-10} only.[1] In the case of gold nanostructures, an additional channel of radiative emission is opened with the transient excitation of a localized plasmon as an intermediate step.[4−6] This plasmon-assisted process is by orders of magnitude more favorable than the direct radiative recombination of a d-band hole with an sp-electron, and hence the luminescence yield is increased by orders of magnitude in the case of gold nanoparticles.[3,5,7−16] Therefore, and because luminescence from gold nanostructures does not suffer from irreversible photobleaching,[17] gold nanoparticles bear huge potential as dyes in bioimaging[18,19] or for optical data storage.[20] Reports on PL from individual nanoparticles with various shapes comprise nanorods,[8] nanocubes,[19] nanobipyramids (BPs),[16,21,22] and nanostars.[22] Studies on PL from plasmonically coupled pairs (sometimes trimers) of nanoparticles are so far limited to lithographically fabricated dimers[23−28] or pairs of spherical nanoparticles formed in solution with fixed interparticle distances.[29−31] Alternatively, the PL from gold nanoparticles with localized plasmons

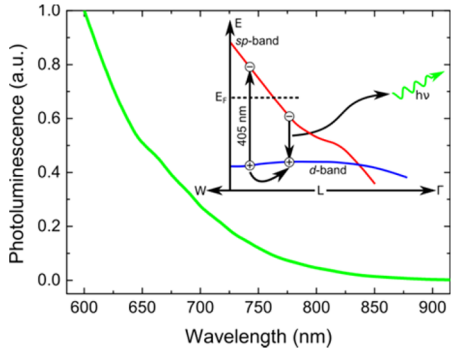

Figure 1. Photoluminescence of gold. Experimental PL spectrum of a gold thin film, excited at 405 nm. (Inset) PL from bulk gold evolves from a three-step process: A d-band hole is created via 405 nm excitation, scatters within the d-band to a state below filled sp-band states, and subsequently recombines radiatively with an sp-electron.

Received: August 24, 2016
Revised: October 1, 2016
Published: October 4, 2016

DOI: 10.1021/acs.nanolett.6b03562
Nano Lett. 2016, 16, 7203−7209

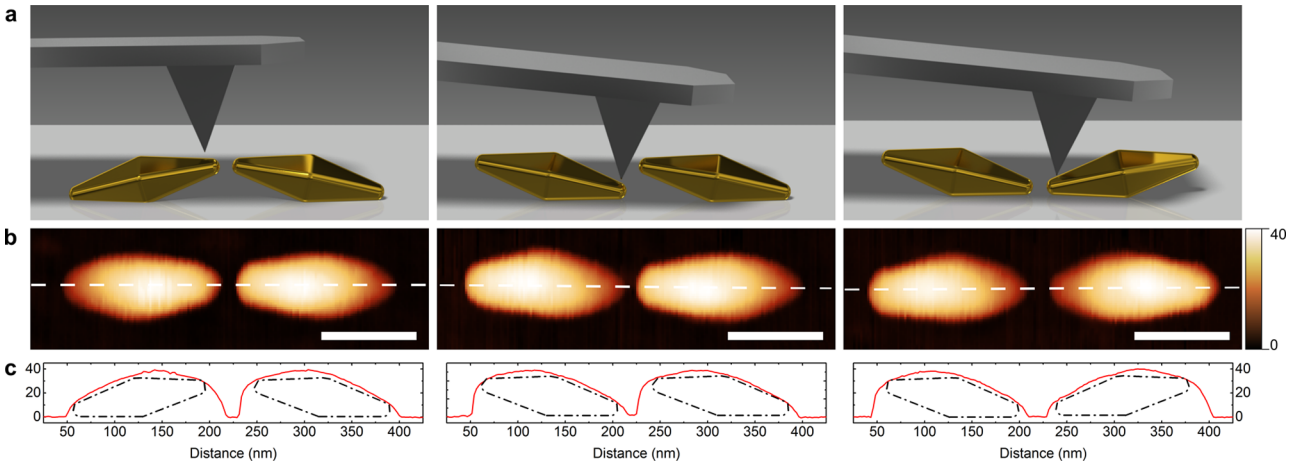

Figure 2. AFM nanomanipulation of dimers of bipyramids: (a) Schematic picture of the bipyramid dimers in the three configurations of facing tip positions (from left to right): Up−Up, Up−Down, and Down−Down. (b) AFM topography images of the three configurations and (c) the height profiles along the dimer axis (marked as white dashed line in the corresponding topography images). The length of the scale bar is 100 nm.

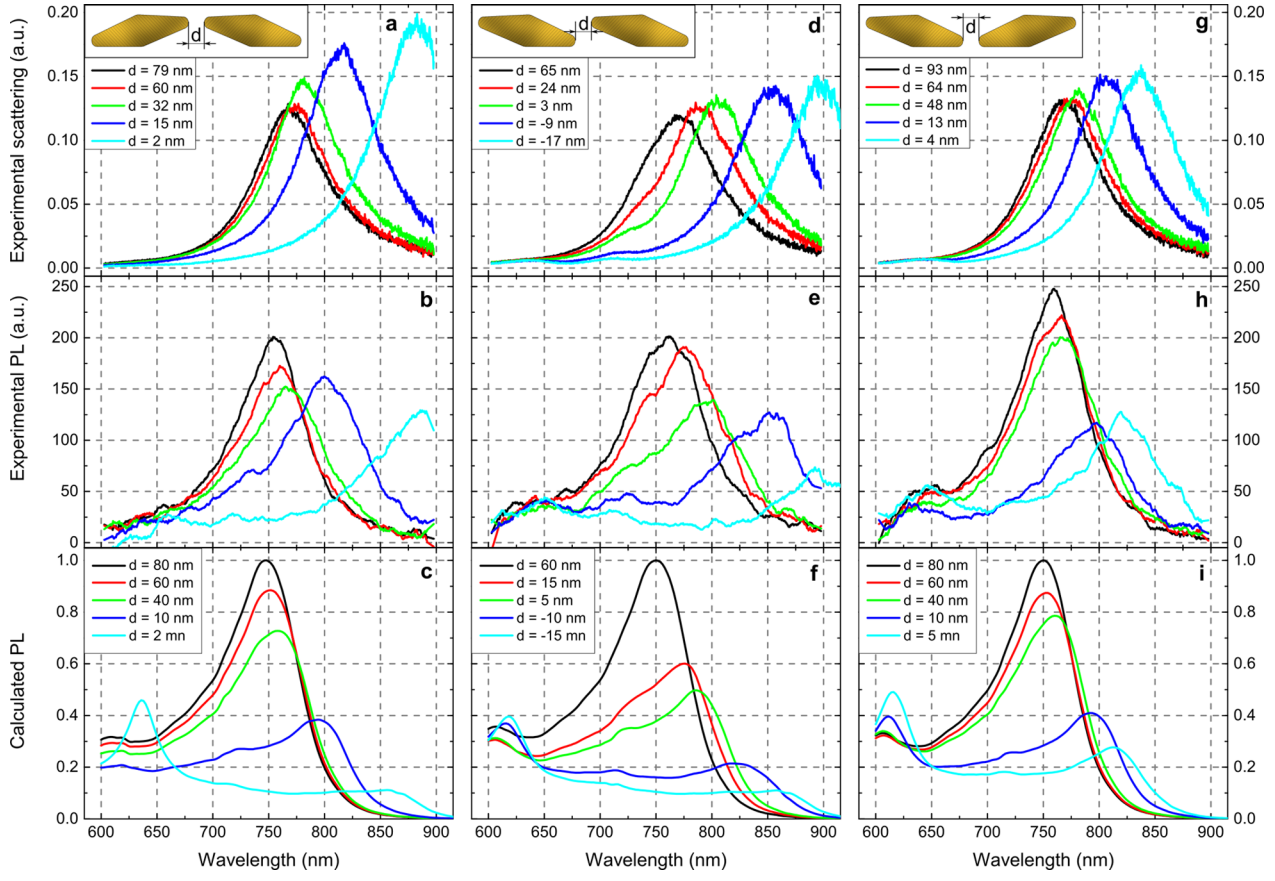

Figure 3. Scattering and photoluminescence from an individual dimer of BPs at different separations *d* and tip orientations: Experimental (a) scattering and (b) PL spectra of the bipyramid dimer in the Up−Up configuration (inset) at different interparticle distances *d* ranging from 79 nm (black) to 2 nm (cyan). (c) Calculated PL spectra of the dimer in the Up−Up configurations with similar interparticle distances as in the experiments. (d−f) The same as (a−c) but for Up−Down configuration. Note that in this configuration the interparticle distance *d* can become negative. (g−i) The same as (a−c) but for Down−Down configuration.

coupling to propagating plasmons of a thin gold film at a fixed distance was investigated.[32,33]

Rash explanations for the impressive enhancement of the PL efficiency in the case of nanostructures compared to bulk gold are commonly given by arguing that the PL from gold is substantially enhanced for those wavelengths, where the PL emission wavelength coincides with the Mie-scattering spectrum of the nanostructures or, in the case of assemblies of nanoparticles, where the hot-spots between the nanoparticles spectrally fit the PL in a similar way, as an increased hot-spot intensity enhances Raman scattering, coupling to fluorophores, or enables nonlinearities.[34,35] However, some experimental reports gave hints that such explanations are premature. For instance, Mohamed et al. observed that the redshift of the

DOI: 10.1021/acs.nanolett.6b03562
Nano Lett. 2016, 16, 7203−7209

extinction spectrum of gold nanorods with increasing rod length is much more pronounced than the redshift of the PL.[8] Further, it was recognized that a redshift of the scattering spectrum (due to gradual changes in geometry of gold nanostructures) is associated with a decrease of the PL intensity, while the scattering intensity increases[15,25,33] and while the absorption strength remains largely unchanged.[30] Only recently, it was pointed out by Lumdee et al.[32] and Andersen et al.[33] (following original ideas from Boyd et al.[3]) that the PL yield should follow the integral of the electric field squared inside the gold nanostructures as well as the gold-intrinsic d-hole recombination rate rather than scattering strengths or hot-spot intensities. However, their experiments were restricted to a single distance between a localized particle plasmon and a thin film surface plasmon.

In this Letter, we systematically investigate the PL from one and the same pair of BPs for different tip-to-tip distances, which is manipulated with nanometer accuracy using the cantilever of an atomic force microscope (AFM). We find that the PL redshifts and diminishes with decreasing tip-to-tip distance, which is in good agreement with numerical simulations considering the gold-intrinsic d-hole recombination strength and the electric field inside the BPs, not only for the fundamental in-phase dipole coupling between the two BPs, but also for higher order coupled plasmonic modes, which to the best of our knowledge has not been observed in such detail before.

We used the cantilever of the AFM to mechanically position[37−40] two nearly identical BPs, so that the BPs are aligned collinearly along their long axes and we subsequently varied the tip-to-tip distance between the BPs. This allows for varying and controlling the distance between the nanoparticles with nm accuracy, which is 1 order of magnitude more precise compared to typical precisions achieved in electron beam lithography.[23,25] In addition, the specific BPs' morphology allows forming dimers in three configurations, namely adjacent tips down (Down−Down), adjacent tips up (Up−Up), or one tip up, one down (Up−Down) (Figure 2a). Figure 2b,c shows AFM-topography images and height profiles, respectively, of the same dimer in the three configurations.

After each manipulation step, the dark-field scattering and PL spectra were taken with an inverted microscope underneath the AFM. Figure 3a shows the measured dark-field scattering spectra of the BP dimer in Up−Up configuration for different interparticle distances d. Details on retrieving interparticle distances can be found in the Supporting Information. Decreasing the interparticle distance leads to a redshift of the scattering spectra and a correlated redshift of the PL spectra (Figure 3b). Nevertheless, the PL is slightly blueshifted with respect to the scattering spectrum[10,15,24,25,30] except for the closest distance. Most interestingly, the PL intensity is significantly decreased for decreasing distances d; this is in contrast to the scattering intensity, which increases with decreasing d.

Figure 3 panels d,e and g,h shows the experimental scattering and the PL spectra in the case of Up−Down and Down−Down geometries, respectively. Note that in the Up−Down case, negative distances are possible[41] and have been realized. Again, the main PL maxima spectrally redshift but become less pronounced with decreasing distance, which is in anticorrelation with the scattering intensity.

In order to gain deeper insights into the anticorrelation between scattering strength and PL amplitude, we calculated the PL of the dimers of BPs using the PL of a smooth film (Figure 1) and the electric field inside the nanoparticles as input. In the case of a two-level system emitting at frequency ω_{em}, Fermi's golden rule tells that the fluorescence emission is proportional to the transition matrix element (an intrinsic feature of the emitter) and the density of electromagnetic states into which the created photons emit. PL from bulk gold is substantially more complicated but still can be sorted into two components, one ($F(\omega_{em})$) representing all material-associated contributions (intrinsic feature of the gold) and one ($G(\omega_{em})$) reflecting the emission of a photon out of the material into free space. $F(\omega_{em})$ is given by[3] $F(\omega_{em}) = D(\omega_{em})\cdot M(\omega_{em})$, whereby $D(\omega_{em})$ reflects the probability that the d-band hole scatters from its original position in k-space at the moment of excitation to a position where the emission of a photon of frequency ω can occur (Figure 1, inset). $M(\omega_{em})$ is proportional to the matrix element of a d-band hole recombining with an sp-band electron, multiplied by the joint densities of the respective holes and electrons.

In the case of bulk metal, the emission factor $G_{em}^{bulk}(\omega_{em},\vec{r}) = L(\omega_{em},\vec{r})\cdot T(\omega_{em})$ represents the probability $L(\omega_{em},\vec{r})$ that the photon travels from the place of origin $\vec{r}$ toward the surface of the metal (given by Lambert−Beer's law) and that it is transmitted through the surface $T(\omega_{em})$ (given by the respective Fresnel coefficient).[3] In order to calculate the external quantum efficiency, which is actually measured, one more term $G_{ex}^{bulk}(\omega_{ex},\vec{r})$ needs to be introduced. It is proportional to the probability that a d-band hole is locally excited at the position $\vec{r}$ via the absorption of a photon of frequency ω_{ex}.

The totally measurable luminescence spectrum $S_{film}(\omega_{em})$ of a smooth gold film is then given by

$$S_{film}(\omega_{em}) = F(\omega_{em}) \int_{film} G_{ex}^{bulk}(\omega_{ex}, \vec{r}) G_{em}^{bulk}(\omega_{em}, \vec{r}) d^3\vec{r} \quad (1)$$

where integration is carried out over the volume of the film.

In the case of PL from a dimer of gold bipyramids, the gold-intrinsic factor $F(\omega_{em})$ will be the same as for smooth films. However, there will be a substantially modified second contribution $G_{em}^{DBP}(\omega_{em},\vec{r})$, including plasmon-enhanced emission of gold fluorescence. Similarly, a plasmon-enhanced excitation of d-band holes will be modified to $G_{ex}^{DBP}(\omega_{ex},\vec{r})$. This leads to the fluorescence spectrum

$$S_{DBP}(\omega_{em}) = F(\omega_{em}) \int_{DBP} G_{ex}^{DBP}(\omega_{ex}, \vec{r}) G_{em}^{DBP}(\omega_{em}, \vec{r}) d^3\vec{r} \quad (2)$$

where integration needs to be carried out over the volume of the dimers of bipyramids (DBP). The integrals over the products $G_{ex}\cdot G_{em}$ in eqs 1 and 2 reflect the probability that a d-band hole is locally created, and the photon created subsequently inside the metal is emitted. For the latter process, the detector is quasi infinitely far away, and largely a plane wave will be detected. Reciprocity predicts that the light emission probability into a certain direction and mode of polarization can be calculated from the integral of the local intensity enhancement induced within the respective volume (film or dimers of BPs) by an incoming plane wave of amplitude E_0 from this direction and of this particular polarization mode.[32,42] Hence, $G_{em}^{i}(\omega_{em},\vec{r}) \propto |E^{i}(\omega_{em}, \vec{r})/E_0(\omega_{em})|^2$ whereby i stands for "bulk" or "DBP" if the field is considered inside the film or the dimer of BPs, respectively. Similarly, the probability that a

DOI: 10.1021/acs.nanolett.6b03562
Nano Lett. 2016, 16, 7203−7209

d-band hole is created at a given point inside the metal follows the proportionality $G^{i}_{ex}(\omega_{ex}, \vec{r}) \propto |E^{i}_{ex}(\omega_{ex}, \vec{r})/E_0(\omega_{ex})|^2$. The PL spectrum of dimers of BPs can thus be calculated from the experimental PL spectrum $S_{film}(\omega_{em})$ of a smooth film (Figure 1) by eliminating $F(\omega_{em})$ in eqs 1 and 2:

$$S^{pred.}_{DBP}(\omega_{em}) \propto S_{film}(\omega_{em}) \frac{\int_{DBP} \left|\frac{E(\omega_{ex},\vec{r})}{E_0(\omega_{ex})}\right|^2 \left|\frac{E(\omega_{em},\vec{r})}{E_0(\omega_{em})}\right|^2 d^3\vec{r}}{\int_{film} \left|\frac{E(\omega_{ex},\vec{r})}{E_0(\omega_{ex})}\right|^2 \left|\frac{E(\omega_{em},\vec{r})}{E_0(\omega_{em})}\right|^2 d^3\vec{r}} \quad (3)$$

The integrals were evaluated numerically using the Comsol Wave Optics package in frequency domain. The spectra of the calculated PL (polarized 1:10^{-3} along the dimer-axis, which is in accord with previous experimental findings[43]) are shown in Figure 3c,f,i and reproduce the trend that the PL intensity generally decays with decreasing tip-to-tip distance as shown by the measured spectra in Figures 3b,e,h in Up−Up, Up−Down, and Down−Down configurations, respectively. However, while the general trend is reproduced, the calculations overestimate the weakening of the PL beyond 800 nm. A possible explanation could be that the gold-intrinsic factor $F(\omega_{em})$ is in fact different in the case of gold films and gold nanoparticles for wavelengths above approximately 800 nm. This could be explained by either a change in the density of states for sp-band electrons, or by energetic shifts of the Fermi level, the sp-band, or the d-bands due to quantum confinement; however, we do not expect such effects to be too pronounced in the size range of the bipyramids. It may also be that transitions near the L or the X point of the Brillouin zone couple differently to plasmons in different nanoscale geometries.[44] Finally, some corrugations of the thin film may affect the experimental result for $S_{flim}(\omega_{em})$, while the effect of such corrugations was not included in calculating the integral in eq 1. This would lead to some error for the estimate for $F(\omega_{em})$ and hence to an error in the normalization in eq 3. However, the surface roughness of the gold film was checked with the AFM and found to be ±0.5 nm (standard deviation) only. Further, if such error due to corrugations in the thin film exists, Figure 3 demonstrates that it will affect the results only for wavelengths above 800 nm.

To illustrate the anticorrelation of hot spot intensity with PL, we calculated the electric field enhancement in the center between the two tips, each at the respective wavelength of maximal field enhancement (solid lines in Figure 4). The hot spot intensity increases with decreasing distance d, in contrast to the experimental maximal PL intensity (dots in Figure 4). Examples for an interparticle distance of 5 nm are shown in the supersets of Figure 4, evaluated at the peak wavelength of the coupled plasmon resonances at this distance (800 nm for Up−Down and 830 nm for Up−Up and Down−Down). These results clearly show that the intensity inside hot-spots or, generally, the near field intensity outside the metallic nanoparticles[16,45] cannot predict the amplitude of gold PL in nanostructures in the right way. We note in passing that the tip-to-tip distances are too large in our case (specifically for the Up−Down configuration, but also for basically all cases in Up−Up and Down−Down configuration) for tunneling or nonlocal effects to become relevant.[46]

It was also found by others that neither the scattering intensity[15,25,30] nor the absorption cross section[30] is a trustful measure to predict the redshift-associated decrease of the PL intensity correctly, and more accurate measurements (as they are now available with our nanometer-precise distance control

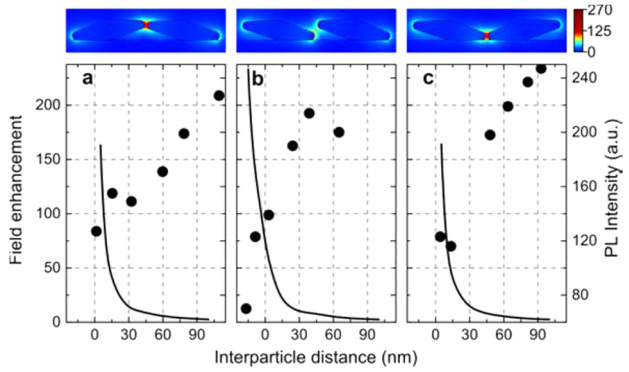

Figure 4. Anticorrelation of the calculated field enhancement $|E/E_0|$ at the center between the two adjacent tips (solid lines) with the measured PL intensity (dots). (a) Up−Up, (b) Up−Down, and (c) Down−Down configuration. Upper panels: Numerically calculated electric field enhancement $|E/E_0|$ relative to the incident field E_0 evaluated at the coupled plasmon resonances (800 nm for Up−Down, 830 nm for Up−Up and Down−Down) for an interparticle distance of 5 nm.

on one and the same BP dimer), as well as a better theory were demanded.[30] For the latter, we argue that eq 3, specifically the integral of the square of the field inside the nanostructure, should be used rather than absorption or scattering cross sections. The absorption cross section is proportional to $\omega_{em}\varepsilon''(\omega_{em}) \int_{DBP} |E(\omega_{em}, \vec{r})|^2 d^3\vec{r}$, which differs from the numerator in eq 3 by a prefactor containing the frequency of the PL emission and the imaginary part of the dielectric function $\varepsilon''(\omega_{em})$. It does not contain the material-intrinsic radiative recombination strength $M(\omega_{em})$ of electrons below the Fermi edge but contains absorption strengths for d-band electrons excited into empty sp-states above the Fermi edge or sp-intraband absorption, both irrelevant for emission. Using the scattering cross section is similarly problematic, as scattering is an elastic process, while PL is not. Almost needless to state is that if absorption and scattering cross sections have no real physical justification to be used to predict PL enhancement, the extinction cross section should not be used either. Nevertheless, previous reports using spectra of near-field enhancement, absorption or scattering retrieved somewhat satisfactory results for the prediction of PL spectra from gold nanostructures, as plasmonic spectra are broad and all these spectra show similarities and also in the current case, the redshift of the PL is well mirrored in the redshift of the scattering intensity (Figure 3). However, they might also differ substantially from each other[45] as well as from the spectral dispersion of the integral over the inside intensity in some cases.

Finally, we would like to turn to the tiny details in the experimental and simulated PL spectra, namely to the spectral shoulders around 725 nm, which are reproduced well in the simulations in all three cases and also to the side maxima around 625 nm, which are present in the simulations, though slightly shifted to shorter wavelengths compared to the experimental results. Those side-maxima are most pronounced in the case of the Up−Down configuration, so we concentrate our discussion on this configuration. Figure 5a shows the experimentally obtained peak positions for all three spectral features as a function of distance d in the Up−Down configuration (obtained by fitting three Lorentzians, see Supporting Information). For clarity, we restricted the number of experimental spectra in Figure 3 to five, but PL spectra for

DOI: 10.1021/acs.nanolett.6b03562
Nano Lett. 2016, 16, 7203−7209

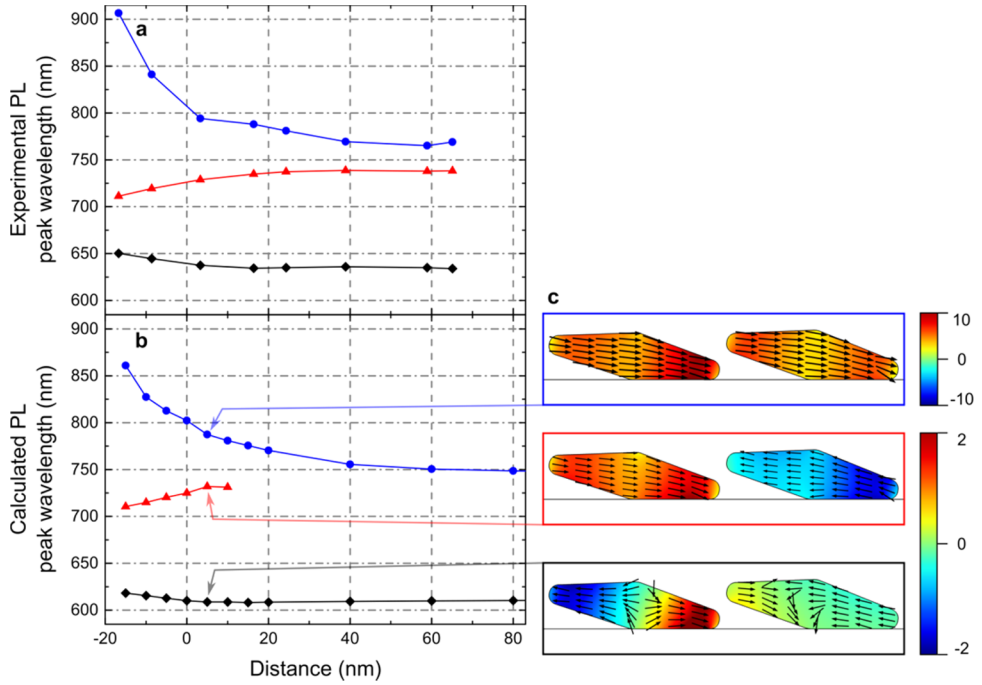

Figure 5. Wavelengths of the maxima of the (a) experimental and (b) calculated PL spectra of the gold BP dimers as a function of interparticle distance for Up−Down configuration. (a) Experimentally measured spectral redshift of the main maximum (750−900 nm, blue dots), the shoulder around 725 nm (red triangles), and the side-maximum around 625 nm. (b) Same as for (a) but now displaying the spectral shift of the calculated PL spectra. (c) Numerical simulations of the electric fields for all three resonances at a distance of 5 nm.

more distances were measured and the positions of the maxima for all experimentally realized distances are shown in Figure 5a. The redshift of the main resonance (blue dots) with decreasing distance, the blueshift of the shoulder around 725 nm (red triangles), and the redshift of the resonance around 625 nm (black diamonds) are clearly visible for the experimental PL spectra (Figure 5a) and nicely reproduced by the calculated PL spectra (Figure 5b) using eq 3. We would like to emphasize that the input for the calculations according to eq 3 was the experimentally determined fluorescence from the film (Figure 1), the tip-to-tip distance as retrieved from the AFM profiles (for details of the retrieval see Section E of the Supporting Information), the geometry of both bipyramids as described in Section D of the Supporting Information, and the dielectric constants taken from literature.[47] There were no free parameters. Hence the agreement between Figure 5 panel a and b is quite remarkable and a further confirmation of eq 3.

The three pictures in Figure 5c show the field distribution inside the Up−Down dimers at a distance of 5 nm. The color scale gives the x (horizontal) component of the electric field, normalized to the incoming field. The arrows (of unit length) show the direction of the field. The longest wavelength resonance (90° out of phase with the incoming field) is clearly identified to be the resonance where both long axes' plasmons of the two BPs couple in phase, resulting in an overall dipolar mode, which redshifts with decreasing distance. The resonance around 725 nm (52° out of phase with the incoming field) can be associated with the same longitudinal plasmons in the BPs but now coupling almost in antiphase. This results in an overall quadrupolar "dark mode", which blueshifts with decreasing tip-to-tip distance.

Indeed, the resonance at 725 nm appears only as a weak shoulder in the PL spectra of Figure 3, as expected for an overall quadrupolar symmetry. For large distances, the interactions of the longitudinal BP plasmons ceases and hence the spectral positions of the in-phase (blue dots) and antiphase (red triangles) converge at around 750 nm, and this is in accord with the single particle resonances shown in Figure S2 in the Supporting Information.

For antiphase coupling (red triangles), the symmetry between both longitudinal dipoles is broken in the case of the Up−Down configuration because the downward-oriented tip experiences a higher refractive index due to the glass substrate than the upward tip. This leads to a stronger field for the downward oriented tip, and the broken symmetry leads to more efficient coupling to far field PL radiation than in the Up−Up or the Down−Down configurations. Indeed, the shoulder around 725 nm is weaker in these two cases (Figure 3) than for the Up−Down configuration. The shortest wavelength resonance around 625 nm (at 72° phase shift compared to the incoming field) is a higher order mode, coupling the two quadrupolar BP modes, and it redshifts with decreasing distance. Indeed, there is a valid question why PL supported by such higher order plasmonic modes couples to the far field at all. One possible reason was already mentioned, and that is the asymmetry of refractive indices for upward tips (facing low-index air as surrounding) and downward tips (facing higher-index glass). The size of the pairs of bipyramids also leads to retardation-induced coupling of quadrupoles to far fields. Further discussion, also including considerations why the PL around 625 nm is sometimes more intense in the calculated spectra than in the measured ones, is left to future investigations.

In summary, we have observed and explained an anti-correlation between the PL from dimers of gold bipyramids with hot-spot intensities or scattering spectra. Signatures of PL enhancement are not only visible for the in-phase coupling of the two longitudinal plasmon resonances but also for the out-

DOI: 10.1021/acs.nanolett.6b03562
Nano Lett. 2016, 16, 7203−7209

of-phase coupling (resulting in an overall quadrupolar behavior) and for a coupled mode of two BP quadrupoles. A theoretical model considering the gold-intrinsic recombination probability of d-band holes and the square of the electric field integrated over the volume of the dimer of bipyramids agrees with the experimental findings. This model (eq 3) can be applied to any other plasmonic structure of nanoscale geometry, as well, but also to other micro- and nanoscale Mie-type resonators, for instance, the recently reported silicon nanoparticles.[48,49] Equation 3 will also remain valid when gold nanostructures are electrically excited in a sort of nanoscale cathodoluminescene[50] or by X-rays[51] if the optical excitation factor $|E(\omega_{ex})/E_0(\omega_{ex})|^2$ is replaced by the respective local excitation probability of d-band holes. Our findings have implications in all cases where the PL from noble metal nanostructures shall be applied, for instance, for biomedical imaging[18,19] or for fluorescent read-out of ultradense, multidimensional data storage.[20] The finding that even quadrupolar plasmonic resonances can support gold-intrinsic PL may trigger further research on the interaction of even higher order multipoles with PL stemming from d-band hole recombination.

Methods. The BPs were wet-chemically synthesized using a seed-mediated-growth method in aqueous solution.[36] Subsequently, the BPs in solution were drop cast on a clean transparent glass substrate. The glass substrate was placed on a three-axis piezo-controlled scanning stage on top of an inverted microscope, carrying a three axes-controlled AFM head (NanoWizard 3, JPK Instruments, Berlin) on top. The side port of the microscope was connected to a spectrometer. This setup allows for simultaneous AFM manipulation, dark-field scattering spectroscopy, and PL spectroscopy. For the latter, a 405 nm CW excitation laser was used. Further details on the experimental setup can be found in the Supporting Information.

■ ASSOCIATED CONTENT

Supporting Information

The Supporting Information is available free of charge on the ACS Publications website at DOI: 10.1021/acs.nanolett.6b03562.

More details on experimental methods and experimental setup; individual AFM and optical characterization of the two bipyramids later used to assemble the pair of bipyramids; retrieval of the geometric parameters of the bipyramids and deconvolution of the tip-to-tip distances; method of retrieval of PL side peaks (PDF)

■ AUTHOR INFORMATION

Corresponding Author

*E-mail: calin.hrelescu@jku.at.

Notes

The authors declare no competing financial interest.

■ ACKNOWLEDGMENTS

The authors cordially thank Jochen Feldmann, Frank Jäckel, and Johannes Ziegler for fruitful discussions, Heidi Piglmayer-Brezina, Habed Habibzadeh, and Alfred Nimmervoll for technical support, and acknowledge financial support by the European Research Council (ERC Starting Grant 257158 "Active NP") and by the Austrian Klima- und Energiefonds (SolarTrap, Grant 843929). B.M. acknowledges financial support by the Erasmus Mundus Mobility Project GATE.

■ REFERENCES

(1) Mooradian, A. *Phys. Rev. Lett.* **1969**, *22*, 185−187.
(2) Apell, P.; Monreal, R.; Lundqvist, S. *Phys. Scr.* **1988**, *38* (2), 174.
(3) Boyd, G. T.; Yu, Z. H.; Shen, Y. R. *Phys. Rev. B: Condens. Matter Mater. Phys.* **1986**, *33* (12), 7923−7936.
(4) Shahbazyan, T. V.; Perakis, I. E.; Bigot, J.-Y. *Phys. Rev. Lett.* **1998**, *81* (15), 3120−3123.
(5) Dulkeith, E.; Niedereichholz, T.; Klar, T. A.; Feldmann, J.; von Plessen, G.; Gittins, D. I.; Mayya, K. S.; Caruso, F. *Phys. Rev. B: Condens. Matter Mater. Phys.* **2004**, *70* (20), 205424.
(6) Shahbazyan, T. V. *Nano Lett.* **2013**, *13* (1), 194−198.
(7) Wilcoxon, J. P.; Martin, J. E.; Parsapour, F.; Wiedenman, B.; Kelley, D. F. *J. Chem. Phys.* **1998**, *108* (21), 9137−9143.
(8) Mohamed, M. B.; Volkov, V.; Link, S.; El-Sayed, M. A. *Chem. Phys. Lett.* **2000**, *317* (6), 517−523.
(9) Varnavski, O. P.; Mohamed, M. B.; El-Sayed, M. A.; Goodson, T. *J. Phys. Chem. B* **2003**, *107* (14), 3101−3104.
(10) Beversluis, M. R.; Bouhelier, A.; Novotny, L. *Phys. Rev. B: Condens. Matter Mater. Phys.* **2003**, *68* (11), 115433.
(11) Bouhelier, A.; Bachelot, R.; Lerondel, G.; Kostcheev, S.; Royer, P.; Wiederrecht, G. P. *Phys. Rev. Lett.* **2005**, *95* (26), 267405.
(12) Eustis, S.; El-Sayed, M. *J. Phys. Chem. B* **2005**, *109*, 16350−16356.
(13) Gaiduk, A.; Yorulmaz, M.; Orrit, M. *ChemPhysChem* **2011**, *12*, 1536−1541.
(14) Yorulmaz, M.; Khatua, S.; Zijlstra, P.; Gaiduk, A.; Orrit, M. *Nano Lett.* **2012**, *12* (8), 4385−4391.
(15) Fang, Y.; Chang, W.-S.; Willingham, B.; Swanglap, P.; Dominguez-Medina, S.; Link, S. *ACS Nano* **2012**, *6* (8), 7177−7184.
(16) Rao, W.; Li, Q.; Wang, Y.; Li, T.; Wu, L. *ACS Nano* **2015**, *9* (3), 2783−2791.
(17) Geddes, C. D.; Parfenov, A.; Gryczynski, I.; Lakowicz, J. R. *Chem. Phys. Lett.* **2003**, *380* (3−4), 269−272.
(18) He, H.; Xie, C.; Ren, J. *Anal. Chem.* **2008**, *80* (15), 5951−5957.
(19) Wu, X.; Ming, T.; Wang, X.; Wang, P.; Wang, J.; Chen, J. *ACS Nano* **2010**, *4* (1), 113−120.
(20) Zijlstra, P.; Chon, J. W. M.; Gu, M. *Nature* **2009**, *459*, 410−413.
(21) Zhang, T.; Shen, H.; Lu, G.; Liu, J.; He, Y.; Wang, Y.; Gong, Q. *Adv. Opt. Mater.* **2013**, *1* (4), 335−342.
(22) Loumaigne, M.; Navarro, J. R. G.; Parola, S.; Werts, M. H. V.; Débarre, A. *Nanoscale* **2015**, *7* (19), 9013−9024.
(23) Schuck, P. J.; Fromm, D. P.; Sundaramurthy, A.; Kino, G. S.; Moerner, W. E. *Phys. Rev. Lett.* **2005**, *94* (1), 17402.
(24) Wissert, M. D.; Ilin, K. S.; Siegel, M.; Lemmer, U.; Eisler, H.-J. *Nano Lett.* **2010**, *10* (10), 4161−4165.
(25) Hu, H.; Duan, H.; Yang, J. K. W.; Shen, Z. X. *ACS Nano* **2012**, *6* (11), 10147−10155.
(26) Walsh, G. F.; Negro, L. D. *Nano Lett.* **2013**, *13* (2), 786−792.
(27) Biagioni, P.; Brida, D.; Huang, J.-S.; Kern, J.; Duo, L.; Hecht, B.; Finazzi, M.; Cerullo, G. *Nano Lett.* **2012**, *12*, 2941−2947.
(28) Yin, T.; Dong, Z.; Jiang, L.; Zhang, L.; Hu, H.; Qiu, C.-W.; Yang, J. K. W.; Shen, Z. X. *ACS Photonics* **2016**, *3* (6), 979−984.
(29) Guan, Z.; Gao, N.; Jiang, X.-F.; Yuan, P.; Han, F.; Xu, Q.-H. *J. Am. Chem. Soc.* **2013**, *135*, 7272−7277.
(30) Huang, D.; Byers, C. P.; Wang, L.-Y.; Hoggard, A.; Hoener, B.; Dominguez-Medina, S.; Chen, S.; Chang, W.-S.; Landes, C. F.; Link, S. *ACS Nano* **2015**, *9* (7), 7072−7079.
(31) Garai, M.; Zhang, T.; Gao, N.; Zhu, H.; Xu, Q.-H. *J. Phys. Chem. C* **2016**, *120* (21), 11621−11630.
(32) Lumdee, C.; Yun, B.; Kik, P. G. *ACS Photonics* **2014**, *1* (11), 1224−1230.
(33) Andersen, S. K. H.; Pors, A.; Bozhevolnyi, S. I. *ACS Photonics* **2015**, *2*, 432−438.
(34) Moskovits, M. *Rev. Mod. Phys.* **1985**, *57*, 783−826.
(35) Hanke, T.; Krauss, G.; Träutlein, D.; Wild, B.; Bratschitsch, R.; Leitenstorfer, A. *Phys. Rev. Lett.* **2009**, *103* (25), 257404.
(36) Liu; Guyot-Sionnest, P. *J. Phys. Chem. B* **2005**, *109* (47), 22192−22200.

DOI: 10.1021/acs.nanolett.6b03562
Nano Lett. 2016, 16, 7203−7209

(37) Schaefer, D. M.; Reifenberger, R.; Patil, A.; Andres, R. P. *Appl. Phys. Lett.* **1995**, *66*, 1012.
(38) Junno, T.; Deppert, K.; Montelius, L.; Samuelson, L. *Appl. Phys. Lett.* **1995**, *66*, 3627−3629.
(39) Hansen, L. T.; Kühle, A.; Sørensen, A. H.; Bohr, J.; Lindelof, P. E. *Nanotechnology* **1998**, *9* (4), 337.
(40) Bek, A.; Jansen, R.; Ringler, M.; Mayilo, S.; Klar, T. A.; Feldmann, J. *Nano Lett.* **2008**, *8* (2), 485−490.
(41) Malachosky, E. W.; Guyot-Sionnest, P. *J. Phys. Chem. C* **2014**, *118*, 6405−6412.
(42) Ding, B.; Hrelescu, C.; Arnold, N.; Isic, G.; Klar, T. A. *Nano Lett.* **2013**, *13*, 378−386.
(43) Wang, Y.; Li, Q.; Rao, W.; Wu, L. *Opt. Commun.* **2015**, *350*, 56−62.
(44) Imura, K.; Okamoto, H. *J. Phys. Chem. C* **2009**, *113*, 11756−11759.
(45) Messinger, B. J.; von Raben, K. U.; Chang, R. K.; Barber, P. W. *Phys. Rev. B: Condens. Matter Mater. Phys.* **1981**, *24*, 649−657.
(46) Kravtsov, V.; Berweger, S.; Atkin, J. M.; Raschke, M. B. *Nano Lett.* **2014**, *14*, 5270−5275.
(47) Johnson, P. B.; Christy, R. W. *Phys. Rev. B* **1972**, *6* (12), 4370−4379.
(48) Evlyukhin, A. B.; Reinhardt, C.; Seidel, A.; Luk̀yanchuk, B. S.; Chichkov, B. N. *Phys. Rev. B: Condens. Matter Mater. Phys.* **2010**, *82*, 45404.
(49) Evlyukhin, A. B.; Novikov, S. M.; Zywietz, U.; Eriksen, R. L.; Reinhardt, C.; Bozhevolnyi, S. I.; Chichkov, B. N. *Nano Lett.* **2012**, *12*, 3749−3755.
(50) Crowell, J.; Ritchie, R. H. *Phys. Rev.* **1968**, *172* (2), 436−440.
(51) Kokkinakis, T.; Alexopoulos, K. *Phys. Rev. Lett.* **1972**, *28* (25), 1632−1634.

DOI: 10.1021/acs.nanolett.6b03562
Nano Lett. 2016, 16, 7203−7209

Anticorrelation of photoluminescence from gold nanoparticle dimers with hot-spot intensity

*Dmitry Sivun, Cynthia Vidal, Battulga Munkhbat, Nikita Arnold, Thomas A. Klar, and Calin Hrelescu**

Institute of Applied Physics, Johannes Kepler University Linz, 4040 Linz, Austria

*calin.hrelescu@jku.at

Supporting Information

A) Experimental setup

The experimental setup is shown in Figure S1. All optical measurements are carried out on an inverted optical microscope Olympus IX-71. The microscope was modified in order to have a simultaneous access to darkfield scattering measurements (Schott KL1500 lamps were used as a source), and photoluminescence measurements. The excitation source for photoluminescence measurements was a 405 nm linearly polarized continuous wave laser (LDH-D-C-405) from PicoQuant providing an intensity of $I \approx 6$ kW/cm² in the focal area. The linear polarization was along the long axes (and the connecting axis) of the BP dimers. Excitation and detection were performed by the same UPLSAPO 40x (NA = 0.95) Olympus objective lens. The scattered or PL light was coupled to a 105 µm core fiber, spectrally dispersed by a Zolix Omni-λ3006 spectrometer and detected by a CCD (Andor iDUS 420). The manipulation steps and topography measurements were carried out by an atomic force microscope (JPK Instruments, NanoWizard 3)

placed on top of the inverted microscope. For both, shifting and seesawing the BPs, AFM probes from Nanosensors (model: PPP-FMR) were used with a force constant around C = 3 N/m. The sample stage and the AFM head each have their separate, three axis piezo control with capacitive feedback.

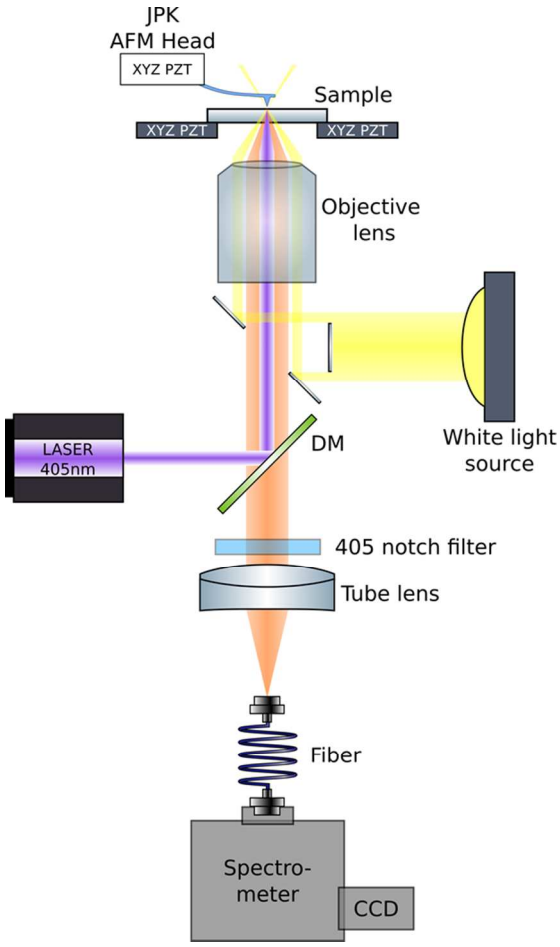

Figure S1. Scheme of the experimental setup**.**

B) Characterization of single bipyramids

Before forming a dimer, two bipyramids with similar scattering signals where identified using dark field scattering spectroscopy. At that time, the individual BPs where well separated, so that the single particle spectra where not compromised by electromagnetic coupling to other particles.

First, the topography was imaged using tapping mode AFM, which proved that the NPs are indeed bipyramids, as well as that the surrounding of the BPs is clear of any other particles (Inset of Figures S2 a,b). In fact, Figures S2 a and b show the scattering and PL spectra of exactly those two NPs that where later nanomanipulated to form the dimer used in the experiments described in the main text (Figures 3,4).

The single BP photoluminescence is always blueshifted compared to the scattering spectra, with a blueshift ranging from 8 to 10 nm. Additionally, there is a clear asymmetry in the photoluminescence spectra, where the signal at short wavelengths is more pronounced than the signal at long wavelengths, similar to what is observed for dimers, see main text.

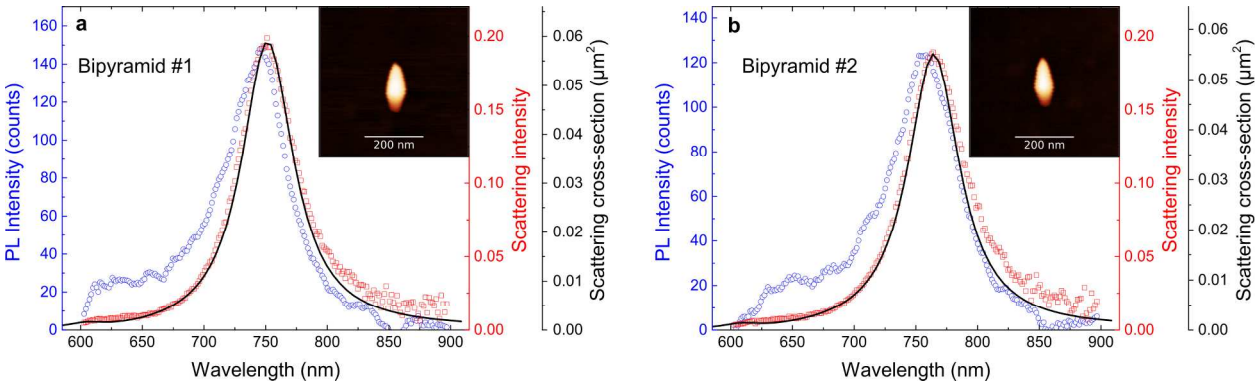

Figure S2. Optical characteristics of the two BPs before forming the dimer used in experiments described in the main text. Open red squares and blue circles correspond to experimentally measured scattering and photoluminescence (PL) spectra, respectively. Solid black line: numerically calculated scattering cross sections. Insets are AFM images of the two BPs, taken with an AFM in tapping mode.

C) Formation of dimers of bipyramids

The two BPs characterized in section B were mechanically positioned next to each other using AFM nano-manipulation[1–4] and subsequently aligned so that their individual long axes are collinear to form dimers with controlled center-to-center distances. Due to their morphology, especially due to the pentagonal cross-section, individual BPs deposited on a substrate are lying on one of the ten facets so that one BP apex is located on the substrate, while the other BP's tip is pointing upwards. This peculiar property allows us to arrange the two BPs in the dimer in three different configurations while keeping the center-to-center distance between the two BPs constant. In contrast to other reports on the scattering of dimers consisting of BPs, where several dimers were formed in solution with fixed apex-to-apex distances and subsequently spin cast on a substrate,[5] our approach allows to investigate the same pair of BPs at different distances from each other and in the three different tip-configurations. We denote the configurations corresponding to the vertical positions of the two BPs' tips pointing towards each other in the dimer as Up-Up, Up-Down and Down-Down, respectively.

D) Retrieval of geometric parameters for simulations

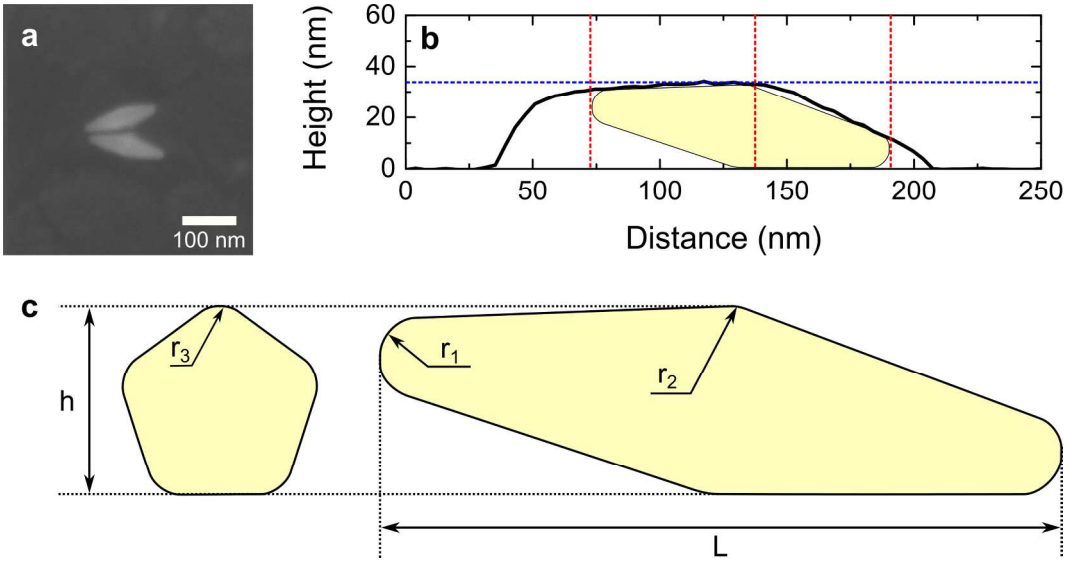

Figure S3. a) SEM image of two BPs from the same batch of BPs as used in the experiment. b) Cross section from an AFM image (Inset in Figure S2a), from which the height of the BP was retrieved as well as other geometrical parameters needed for calculating the geometry and interparticle distance. c) Geometrical parameters of a BP used in numerical simulation. L is the length of a BP, h is the height and r_1, r_2, and r_3 are radii of curvature introduced in order to smooth edges.

All simulations were performed in frequency domain with the commercial finite element solver COMSOL™ , version 4.4, using the Wave Optics package. The polarization of the incident electric field was always parallel to the long axis of a bipyramid dimer axis, and normal incidence was assumed. The dielectric function of gold was taken from Johnson and Christy[6]. The simulation model consisted of a glass substrate with refractive index n = 1.523, topped with bipyramidal NPs, and air with n = 1. First of all a single bipyramid was simulated with geometrical parameters taken from SEM and AFM measurements (Fig. S3 a,b and inset of Fig. S2). The SEM image gives an approximate number for the length L and the angle of inclination

of the BPs, while the AFM measurements revealed the absolute height h. In order to fit the simulated scattering spectra to the experimental ones, the length of the BP model was fine-tuned. The final geometrical parameters retrieved for the two BPs used to form the dimer in the main text are: L = 122.6 nm and h = 35.3 nm for the first BP and L = 121.8 nm and h = 33.5 nm for the second BP. Note that the calculations were carried out respecting this tiny difference in the size of the two BPs. For both BPs, the radii of curvature of the tips, as well as radii of edge smoothing (Fig. S3c) were $r_1 = r_3 = 6$ nm, and $r_2 = 12$ nm, respectively (Fig. S3 c).

E) Tip Deconvolution

In order to be able to retrieve the interparticle distance from AFM topography measurements, the profile of the AFM tip and the profile of BPs need to be deconvolved. This way, it is possible to retrieve the real geometrical parameters of a dimer of BPs from the measured AFM topography. There are several reports dedicated to this problem,[2,7] but these describe only the case of symmetric particles like spheres. In case of BPs lying on one of the facets, the structure is asymmetric, and the convolution near the upper tip of a BP is different from the convolution near the lower tip of a BP.

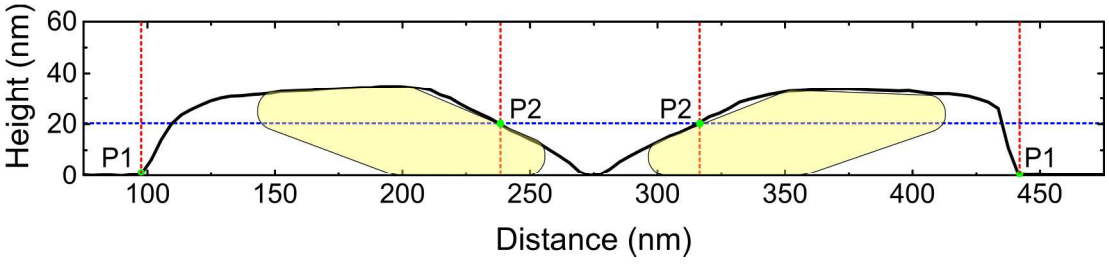

Figure S4. Topographical height profile of the BPs dimer. The black line is the measured height profile. The yellow bipyramids show the assumed positions of the BPs.

Figure S4 shows a height profile obtained from an AFM topography image of a BP dimer. The solid black line is a measured height profile, the yellow BPs fitted inside of it is the profile of the BP used for simulation. As we can see from figure S4, the tip-convoluted lengths of the BPs appear much longer than the real length L, and convolution of the AFM tip is much more pronounced on the side of the upper tip. Even worse, the convolution with the AFM tip could change during experiments (i.e. after some manipulation steps due to slight changes of the tip profile). Therefore, the determination of the distance between BPs is not possible using points P1 in Fig. S4. Generally, one can expect an increase of the convolution with the AFM tip with an increase of the number of manipulation steps, which will lead to a growing error in the interparticle distance in such case. In order to avoid this error, we measure the interparticle distance at convolution-free points of the height profile. Such points are for example the points P2 where the inclined slope of the tips reaches a certain height (e.g. 20 nm, dashed blue horizontal line), as height measurements are by far more accurate in AFM than lateral measurements. The closest position of such selected points, which could be achieved during nanomanipulation, determines the zero distance (d=0).

F) Retrieval of positions of PL side peaks, supported by higher order plasmons:

Three Lorentzians were fit in order to get the positions of the main peak and two weaker signatures in the photoluminescence spectra. As a Lorentzian is well defined in energy rather than wavelength space, the abscissas were first converted to energy scale. Then three Lorentzian curves were fit. One example of fitting is illustrated in figure S5. The obtained peak positions where then calculated back to wavelengths in order to obtain the data shown in figure 5 of the main text.

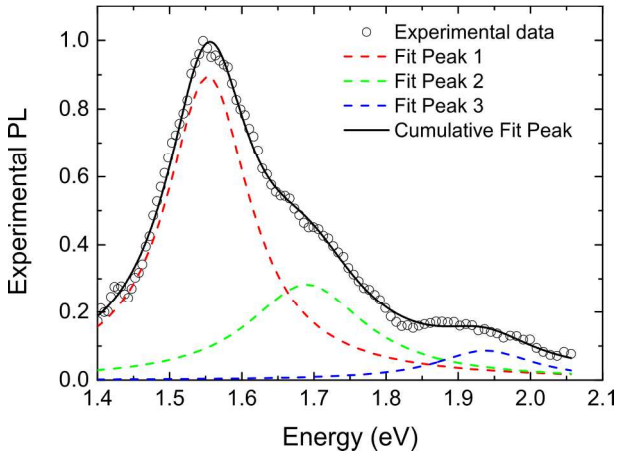

Figure S5: Black open circles show experimentally measured PL- spectra for the Up-Down configuration and an interparticle distance d = 3nm. Red, green, and blue dashed lines indicate the Lorentzian fits for dipolar, quadrupolar, and higher order plasmonic modes respectively. The black solid line shows the cumulative fit.

References

(1) Schaefer, D. M.; Reifenberger, R.; Patil, A.; Andres, R. P. *Appl. Phys. Lett.* **1995**, *66*, 1012.
(2) Junno, T.; Deppert, K.; Montelius, L.; Samuelson, L. *Appl. Phys. Lett.* **1995**, *66*, 3627–3629.
(3) Hansen, L. T.; Kühle, A.; Sørensen, A. H.; Bohr, J.; Lindelof, P. E. *Nanotechnology* **1998**, *9* (4), 337.
(4) Bek, A.; Jansen, R.; Ringler, M.; Mayilo, S.; Klar, T. A.; Feldmann, J. *Nano Lett.* **2008**, *8*, 485–490.
(5) Malachosky, E. W.; Guyot-Sionnest, P. *J. Phys. Chem. C* **2014**, *118* (12), 6405–6412.
(6) Johnson, P. B.; Christy, R. W. *Phys. Rev. B* **1972**, *6* (12), 4370–4379.
(7) Kim, S.; Shafiei, F.; Ratchford, D.; Li, X. *Nanotechnology* **2011**, *22* (11), 115301.